The effect of rear earth doping CdS nanostructure on structural, optical and photoconductivity properties

Ali A. Safi and Isam M. Ibrahim

Department of Physics, College of Science, University of Baghdad

E-mail: dr.issamiq@gmail.com

Abstract

Rare earth elements (Cerium, Lanthanum and Neodymium) doped CdS thin films are prepared using the chemical Spray Pyrolysis Method with temperature 200 ^{o}C. The X-ray diffraction (XRD) analysis refers that pure CdS and CdS:Ce, CdS:La and CdS:Nd thin films showed the hexagonal crystalline phase. The crystallite size determined by the Debye-Scherrer equation and the range was (35.8–23.76 nm), and it was confirmed by field emission scanning electron microscopy (FE-SEM). The pure and doped CdS shows a direct band gap (2.57 to 2.72 eV), which was obtained by transmittance. The room-temperature photoluminescence of pure and doped CdS shows large peak at 431 nm, and two small peaks at (530 and 610 nm). The Current – voltage measurement in dark and illumination (100 mW/cm^2, 183 mW/cm^2 and 288 mW/cm^2) condition. The photocurrent increases and the resistivity decreases with the light intensity increases. So film reveals photoconductivity phenomena suggesting it's useful for optoelectronic applications.

تأثير العناصر الأرضية النادرة المشوبة لكبريتيد الكادميوم على الخواص الهيكلية والبصرية والتوصيلية الضوئية.

علي عبد المهدي صافي و عصام محمد إبراهيم

قسم الفيزياء، كلية العلوم، جامعة بغداد

الخلاصة

تم تحضير الاغشية الرقيقة لكبريتيد الكادميوم المطعم بالعناصر الأرضية النادرة عن طريق استخدام طريقة الرش الكيميائي وبدرجة حرارة 200 درجة مئوية. تشير تحليلات الاشعة السينية بأن الطور البلوري للاغشية الرقيقة النقية والمطعمة (CdS, CdS:Ce, CdS:La, CdS:Nd) اتخذت الشكل السداسي. الحجم البلوري تم تحديده بواسطة استخدام معادلة شرر وكان الحجم ضمن المدى (35.8–23.76 nm) ، وقد تم تأكيد ذلك بواسطة (مجال انبعاث المسح المجهري الإلكتروني). CdS النقي والمشوب يظهر فجوة طاقة مباشرة (2.57 الى eV 2.72) والتي تم الحصول عليها عن طريق النفاذية. التلألؤ الضوئي عند درجة حرارة الغرفة يبين قمة كبيرة عند الطول الموجي (431 nm) وقمتين صغيرتين عند (610 nm و 530). تم قياس التيار – فولتية في حالة الظلام والاضاءة عند الشدات الضوئية (288 mW/cm^2 183, 100,)، عند زيادة شدة الضوء يزداد التيار الضوئي وتقل المقاومية. لذا يكشف الفيلم عن ظاهرة التوصيلية الضوئية التي تشير إلى أنه مفيد للتطبيقات الإلكترونية البصرية.

Introduction

Cadmium sulphide consider the most common semiconductor due to its high band gap (2.42 eV) and potential applications in the area of electronic and optoelectronic devices fabrications [1], CdS structure classify in three types are namely hexagonal wurtzite,

high pressure rock-salt phase and cubic zinc blend, the hexagonal wurtzite is important among these because its stability and easily synthesized [2, 3]. Rare earth elements possess interesting optical properties due to their good interaction with light [4-6], and provide significant advantages to semiconductors which are important for photoluminescence and other optical properties, they offer the probability of getting radiation with wavelength for blue, green and red light, which are covering all wavelength for operation the devices. The electronic structure of rare earth elements are the same in their outer of $(5s^2\ 5p^6\ 6s^2)$ and differ only by electrons occupying the inner partially filled $4f$ shell [7], and their ionization occurs when they lose two $6s$ and one $4f$ electrons and form a stable trivalent state [8]. When semiconductor doped with such ions and excitation by suitable wavelengths a sharp line emission will be appears due to the transition of electrons in $4f^n$ shell [9], this line emission covers a wide range of UV, Vis, IR regions of the spectrum. Many papers reported the optical properties of rare earth elements doped CdS which has characteristics thin film, nanoparticles, nanocrystals and nanofilms such as [10 - 15] respectively. In this work we report the effect of (Ce, La and Nd) doping on the structural and optical properties of CdS thin films synthesized by chemical Spray Pyrolysis Method.

Experimental work

The solution used to prepare pure CdS was from cadmium chloride ($CdCl_2.H_2O$) of molecular weight (201.33 g/mol) and purity 99.9%, which is a white crystal fast-soluble in distill water and ethanol as a source of cadmium ion. And use thiourea ($NH_2.SC.NH_2$) of molecular weight (76.12 g/mol) and purity 99.9%, as a source of sulphur ion. Were both Separately dissolved in 40 ml of distilled water and 10 ml ethanol and then mixed the Cadmium chloride solution with Thiourea using a magnetic stirrer with temperature 30^0C for 30 minutes to complete the solubility process and get CdS . The solution was present at a molecular concentration (0.2M). While Cerium Oxide (CeO_2), Lanthanum Oxide (La_2O_3) and Neodymium Oxide (Nd_2O_3) separately dissolved in 40 ml of distilled water and 10 ml ethanol using a magnetic stirrer with temperature $30^{\circ}C$ for 30 minutes, The solutions were present at a molecular concentration (0.2M) and add (5ml) from each one of the deposition to (45ml) of Cd^{+2} ion source deposition and put this mixed on the magnetic stirrer with $30^{\circ}C$ for 30 minute. And the mixture add to 50ml of sulfide in same steps above to get CdS:Ce, CdS:La and CdS:Nd solutions with concentration of doping (10%), glass substrates of dimensions (2.5×1) cm cleaned with distilled water, ethanol and ultrasonic cleaner, silicon substrate of dimensions (1×1) cm cleaned in mixture of (9 ml) distilled water and 1ml of ethanol, after that use air flow at room temperature to drying these substrate. The deposition spray on substrate by Chemical Spray Pyrolysis Method with substrate temperature 200 $^{\circ}C$ and the distance was set as 20 cm between the nozzle and substrates, the growth of samples by rate 0.6 ml/min, This means that it takes about two and a half hours to spray the solution. Aluminum electrodes on the surface of pure and doped CdS thin films had been proceed, this process occurs by thermal evaporation method under vacuum (10^{-5} mbar), using Edward coating unit model (Auto 606).

The structure of deposited thin film has been analysis using X-Ray diffraction, morphology used Field Emission Scanning Electron Microscope (FESEM), to calculate (transmission and optical energy gap (E_g) were studied by Spectrophotometer, photoluminescence of thin films were measured by RF-551 Spectrofluorometric Detector (Shimadzu), photoconductivity and photosensitivity were studied by sensitive digital electrometer type keithly (2400).

Results and discussion

Thin films structural properties were examined by the XRD as shown in Fig.1, and the data of CdS pure and (CdS:Ce, CdS:La and CdS:Nd) at (10%) listed in Table 1. For undoped CdS sample has polycrystalline structure with the reflection planes of (100), (002), (101), (110), (103), and (112), all those reflection planes noted also for CdS:Ce pattern and shows the film exhibited hexagonal (wurtzite) crystal structure as indicated by the absence of characteristic (200) and (311) peaks of the cubic CdS structure, with a preferential orientation along the (002) plane. From the XRD spectra it was also observed that no diffraction peaks corresponding to the impurity phases and for Ce element were detected or secondary phases, which similar to M. Sreenivas et al. [16] and that confirmed the successful incorporation of Ce ions into the crystal lattice of CdS particles [11]. While CdS:La at 10%, noted from this figure the decreasing in diffraction peaks intensities for (100), (002) and (101), while observed increasing in diffraction peaks intensities for (102), (110), (103) and (112), and have preferential orientation along the (112) plane of hexagonal phase and there are no such for

impurity, which is the evidence of successful dissolution of La atoms in host structure. The decreasing and increasing in peaks intensities compare with those of pure CdS refer to the more random preferred orientation takes place [17]. The pattern of CdS:Nd at 10 %, shows that the preferential orientation along the (101) plane of hexagonal phase, which agreement with hexagonal phase structure of CdS (JCPDS File No. 96-101-1055), and observed the increasing in diffraction peaks intensities for (002), (101), (102), (110), (103), (112), (201), (202) and (023). Absence of peaks matching to neodymium oxides and neodymium metal clusters confirms that Nd has entered into CdS matrix without changing the crystal structure [18]. In general the diffraction peaks of doped CdS are shift slightly toward smaller diffraction angle. The average crystallite size calculated by Debye Scherrer's equation [19]:

$$D = (0.89\lambda)/(\beta \cos\theta) \qquad (1)$$

where λ is a wavelength of the X rays, β is the full width at half maximum, and θ is the diffraction angle, the average crystallite size corresponding to the maximum intensity peaks at ($2\theta=26.7571$, $2\theta=26.6650$, $2\theta=51.7881$ and $2\theta=51.7080$) for pure and (Ce, La and Nd) doped CdS thin films at 10%) respectively were found to be (40.6, 31.3, 33.3 and 20.2) nm respectively.

Thin films morphological properties were tested by the FESEM images, Fig.2(a-d) show the images of FESEM for pure CdS and doped CdS:Ce, CdS:La and CdS:Nd at 10 %. Image (a) of pure CdS thin film, grains are somewhat homogeneous in both shape and size and grain boundaries are very clear because of the big grain size where its growth is due to the agglomeration of individual particles, and the surface covered by big grains. For Ce doped CdS as show in image

(b), it is observed the topography is different than that of pure CdS, with a compact and dense structure and better in grain correlation with almost uniform distribution over the surface, and the grain boundaries somewhat disappear significantly, which refer to better for CdS thin films for photovoltaic applications [20], it clearly notes the hexagonal shape of particles and this agreement with Hurma [21]. Image(c) for La doped CdS with ratios of 10 %, it is observed an existing of big grains with noticeable boundaries and the most grains are nearly triangle-like in shape with a small amount of polygon-like

through the surface. It observes that the grains size in this image is bigger than the size in the images of CdS:Ce, it seems that the surface has less roughness of the CdS:La thin film raises and that agrees with S. Yılmaz et al. [17], While Nd doped CdS with ratios of 10% as shown in Fig. 2(d), observed that the grains are big with fewer boundaries in comparison with pure CdS and CdS:La, it is noticeable that the shapes are between a polygon and unrecognizable shapes. The topography of the surface could be described as uniform, continuous, dense and smooth surface morphology.
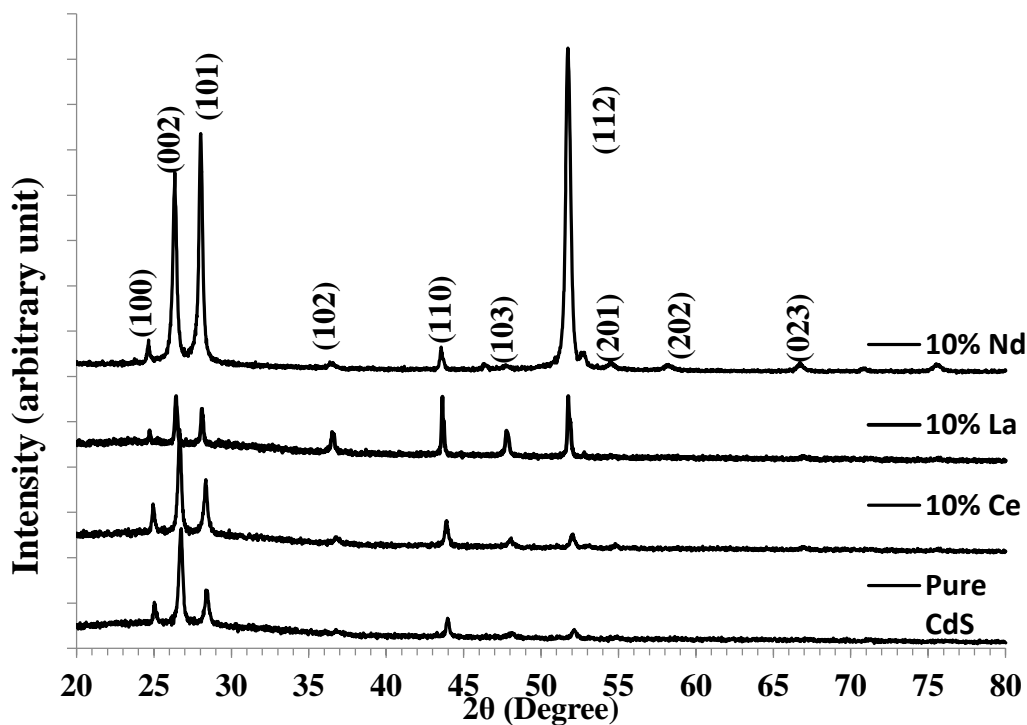

Fig. 1: X-Ray diffraction patterns for pure CdS and (Ce, La and Nd) doped CdS at 10%.

Table 1: Structural parameters for pure CdS and and (Ce, La and Nd) doped CdS at 10%.

Sample	2θ (Deg.)	FWHM (Deg.)	d_{hkl} Exp.(Å)	C.S (nm)	d_{hkl} Std.(Å)	Phase	hkl	card No.
Pure	25.0525	0.1690	3.5516	48.2	3.5940	Hex. CdS	(100)	96-101-1055
	26.7571	0.2010	3.3291	40.6	3.3685	Hex. CdS	(002)	96-101-1055
	28.4310	0.2457	3.1368	33.4	3.1710	Hex. CdS	(101)	96-101-1055
	36.7392	0.2764	2.4443	30.3	2.4577	Hex. CdS	(102)	96-101-1055
	43.9724	0.2457	2.0575	34.9	2.0750	Hex. CdS	(110)	96-101-1055
	48.1495	0.3013	1.8883	28.9	1.9045	Hex. CdS	(103)	96-101-1055
	52.1577	0.3072	1.7522	28.8	1.7667	Hex. CdS	(112)	96-101-1055
	54.8759	0.2764	1.6717	32.4	1.6842	Hex. CdS	(004)	96-101-1055
Ce 10%	24.9450	0.2304	3.5667	35.3	3.5940	Hex. CdS	(100)	96-101-1055
	26.6650	0.2611	3.3404	31.3	3.3685	Hex. CdS	(002)	96-101-1055
	28.3542	0.2610	3.1451	31.4	3.1710	Hex. CdS	(101)	96-101-1055
	36.7699	0.3840	2.4423	21.8	2.4577	Hex. CdS	(102)	96-101-1055
	43.8649	0.3071	2.0623	27.9	2.0750	Hex. CdS	(110)	96-101-1055
	48.0727	0.3379	1.8912	25.7	1.9045	Hex. CdS	(103)	96-101-1055
	52.0502	0.3072	1.7556	28.8	1.7667	Hex. CdS	(112)	96-101-1055
	54.7991	0.3685	1.6739	24.3	1.6842	Hex. CdS	(004)	96-101-1055
	66.9619	0.2918	1.3963	32.6	1.4031	Hex. CdS	(023)	96-101-1055
La 10%	24.7241	0.2207	3.5980	36.9	3.5940	Hex. CdS	(100)	96-101-1055
	26.4459	0.2208	3.3676	37.0	3.3685	Hex. CdS	(002)	96-101-1055
	28.1236	0.2208	3.1704	37.1	3.1710	Hex. CdS	(101)	96-101-1055
	36.6004	0.2649	2.4532	31.6	2.4577	Hex. CdS	(102)	96-101-1055
	43.6203	0.2207	2.0733	38.8	2.0750	Hex. CdS	(110)	96-101-1055
	47.8146	0.2649	1.9008	32.8	1.9045	Hex. CdS	(103)	96-101-1055
	51.7881	0.2649	1.7639	33.3	1.7667	Hex. CdS	(112)	96-101-1055
	66.9757	0.3090	1.3961	30.8	1.4031	Hex. CdS	(023)	96-101-1055
Nd 10%	24.6861	0.2190	3.6035	37.1	3.5940	Hex. CdS	(100)	96-101-1055
	26.3504	0.3065	3.3796	26.6	3.3685	Hex. CdS	(002)	96-101-1055
	28.0584	0.3066	3.1776	26.7	3.1710	Hex. CdS	(101)	96-101-1055
	36.4234	0.5255	2.4647	15.9	2.4577	Hex. CdS	(102)	96-101-1055
	43.5620	0.3065	2.0759	27.9	2.0750	Hex. CdS	(110)	96-101-1055
	51.7080	0.4380	1.7664	20.2	1.7667	Hex. CdS	(112)	96-101-1055
	52.7591	0.3942	1.7337	22.5	1.7363	Hex. CdS	(201)	96-101-1055
	58.1460	0.4818	1.5852	18.9	1.5855	Hex. CdS	(202)	96-101-1055
	66.6861	0.5255	1.4014	18.1	1.4031	Hex. CdS	(023)	96-101-1055

The transmission spectra have been studied by UV-visible spectrophotometer. Fig.3 shows the transmission of pure CdS, CdS:Ce and CdS:La and CdS:Nd at 10%, it is observed that the transmission for samples are high in visible and near IR region, and increases with rare earth elements doping. The enhancement in transmittance value after doped rare earth elements may be ascribed to the grain growth, leading to less grain boundaries and hence less light scattering from the grain boundaries [22]. In general, the values of the transmission are different from rare materials to another doping, where it's are (60%, 90%, 83%, , and 88%) for (CdS, CdS:Ce , CdS:La and CdS:Nd) respectively, that mean highly transparent is found for doped thin film, it can be used in solar cell as transparent window.
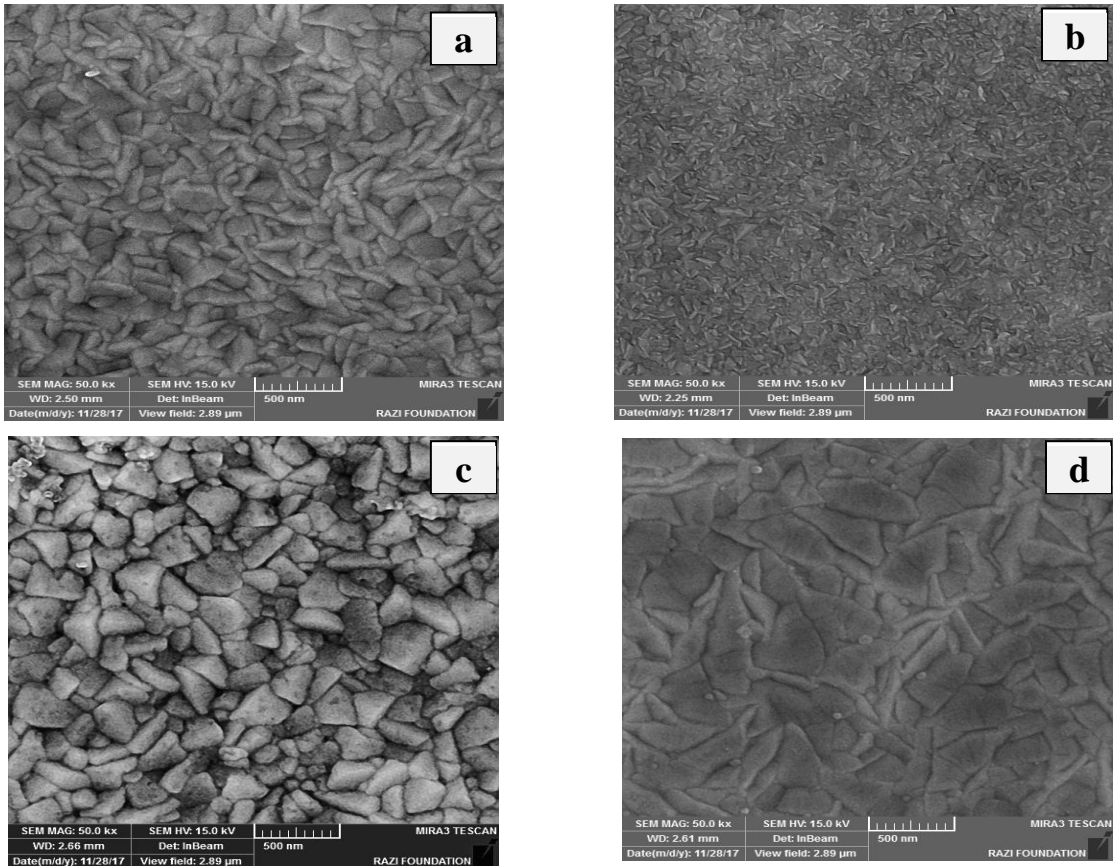
Fig.2: FESEM image of (a) pure CdS (b) CdS:Ce 10 % (c) CdS:La 10 % (d)CdS:Nd 10 %.
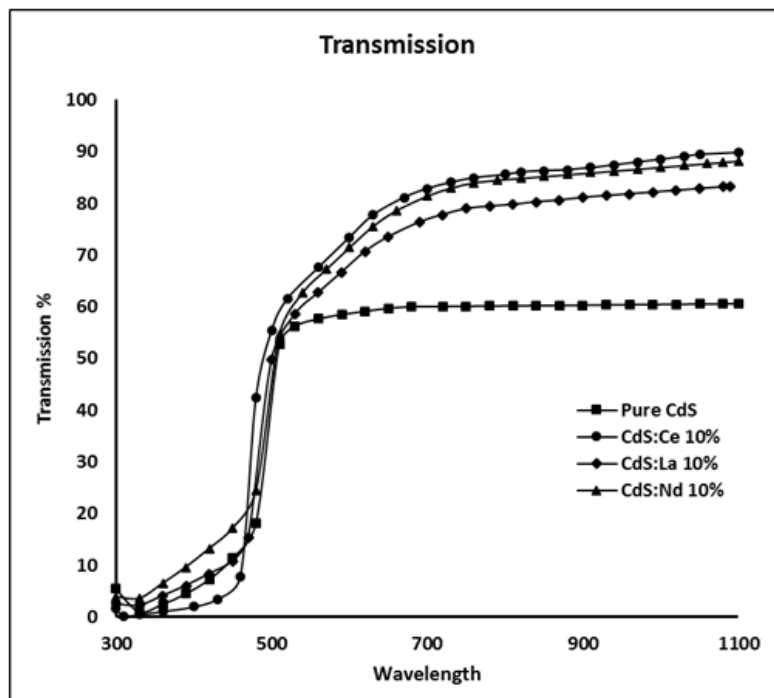

Fig.3: Transmission for pure CdS and (Ce, La and Nd) doped CdS at 10 %.

The optical band gap of the doped and undoped CdS thin films were estimated by Tauc plot as shown in Fig.4. Which it plotted between $(\alpha h\nu)^2$ vs. $(h\nu)$ to gives a straight line indicated to band gap, for pure CdS optical band gap is equal to (2.57 eV), while CdS:Ce, CdS:La and CdS:Nd at (10 %) are equal to (2.65, 2.60 and 2.72 eV) respectively, this increasing in the band gap is due to rearrange the crystalline build that lead to reduction the density of state and the dangling bonds in the band gap, which leads to increasing the band gap [23].

Fig.4: The optical band gap for pure CdS and (Ce, La and Nd) doped CdS at 10 %.

Fig.5 shows the PL results of pure CdS and CdS:Ce, CdS:La and CdS:Nd at ratio (10%) thin films by excited wavelength at 400 nm. For pure CdS there is a broad defect emission because the present of point defects such as cadmium vacancies (V_{Cd}), sulfur vacancies (V_S), cadmium interstitials I_{Cd} and sulphur interstitials (I_S), which act as luminescent centers [24]. It is observed that three beaks, a broad peak between 320 and 480, which centered at 440 nm. The strong PL emission indicates the high crystallinity of CdS sample, and consistent with the XRD results [25], the second peak centered at 530, and the third peak centered at 610 nm, with UV, green and orange emission respectively. The UV emission for the first peak as shown in figure, attributed to transitions from the deep and shallow states [26]. The green emission band of the second peak is due to electronic transition from conduction band to an acceptor level due to interstitial sulphur ions (Is) [27]. The origin of orange band is originating from the transition from the donor levels, created by the occupation interstitial sites of Cd atoms (ICd), to the valence band [18]. Also, it is noted that the peak intensity of CdS:Nd was higher than the CdS:Ce and CdS:La, and that approximate to Shashi et al. [10]
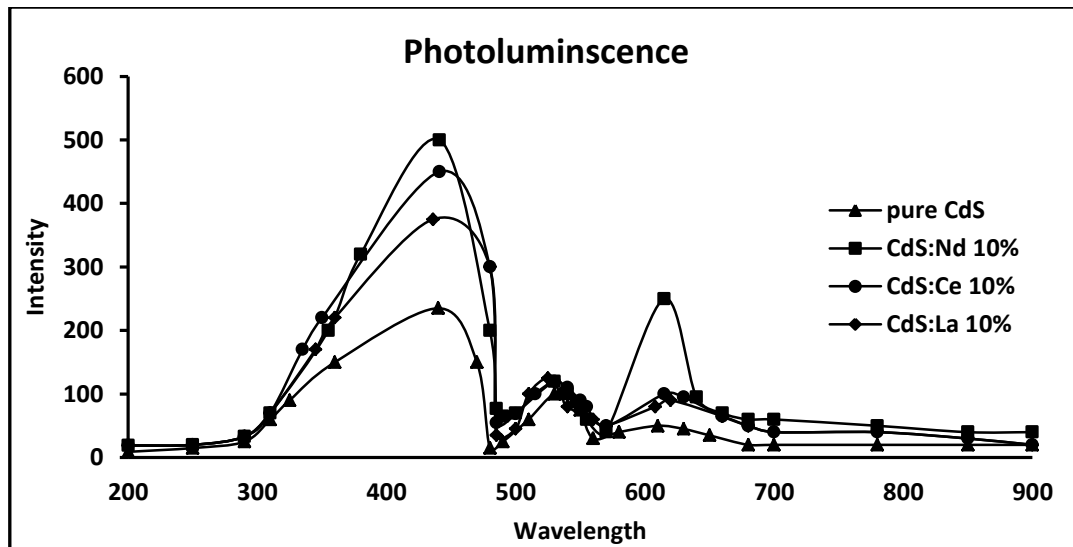
Fig.5: PL spectrum for pure CdS and (Ce, La and Nd) doped CdS at 10 % with excitation wavelength 400 nm.

The current-voltage characteristics as shown in Fig.6 described resultant current in forward and reverse bias in cases of dark for CdS:Ce/p-Si, CdS:La/p-Si and CdS:Nd/p-Si respectively, at 10 %. Fundamentally the dark current under forward bias for pure CdS is generated consequences to the flow of majority carriers, the built-in potential and the width of the depletion layer decrease when the majority carriers injects by the applied voltage, for the low voltage region (0 - 0.4 Volt) the recombination current is generates due to the high concentrations of majority and minority carriers, the little increase in recombination current is noted in case of the low voltage [28]. While in case of a high voltage region (0.4 – 1 Volt), it is observed increase in the current magnitude, this current represent the tunneling current, which has a fast exponential increase due to increase of the voltage, this current called a diffusion current. In case of reverse bias, also there is two regions, for low applied voltage, the current increase slowly, and this current represent generation current, while for high applied voltage, we noted the diffusion current. The magnitude of generation and diffusion current of doped CdS:Ce, CdS:La and CdS:Nd at 10 % were increase compared with pure CdS, where the increasing is associated with increase of the charge carriers concentrations, also the increasing in current density is due to reduce of defects and dislocations which have directly effect on the charge carriers mobility which act as active recombination centers, that leads to increase the current across the junction [29].
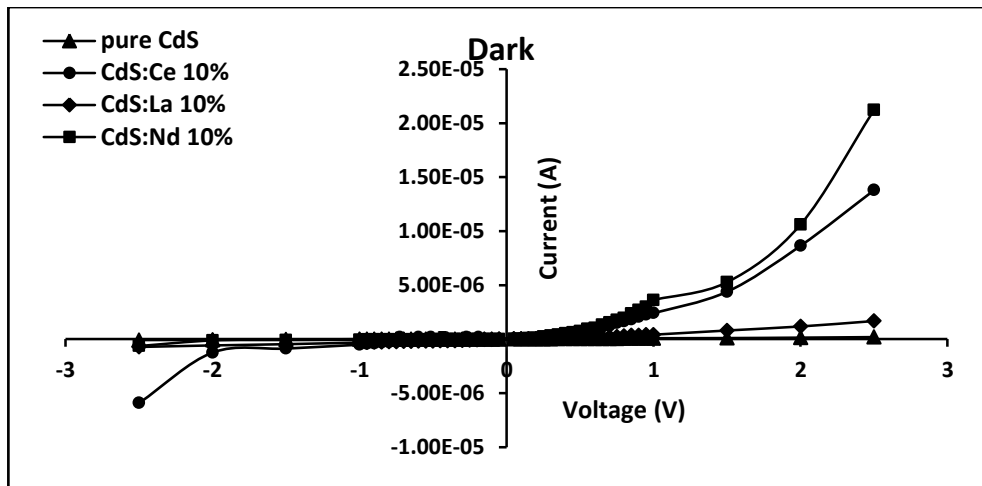
Fig.6: I-V characteristics of CdS and (Ce, La and Nd) doped CdS at 10% in dark condition.

Fig.7 shows the variation of ln(I) and (V) with forward bias for pure CdS and doped CdS:Ce, La and Nd, at 10% under dark, this relation used to determine the ideality factor (β) from the slope at the first region (low region), while the second region (high voltage) or tunneling has been found from the second slope (A_t). The values of (β) and (A_t) for pure CdS and (Ce, La and Nd) doped were found (9.8, 4.95, 8.65 and 2.99) and (38.16, 14.63, 15.13 and 12.29) respectively.
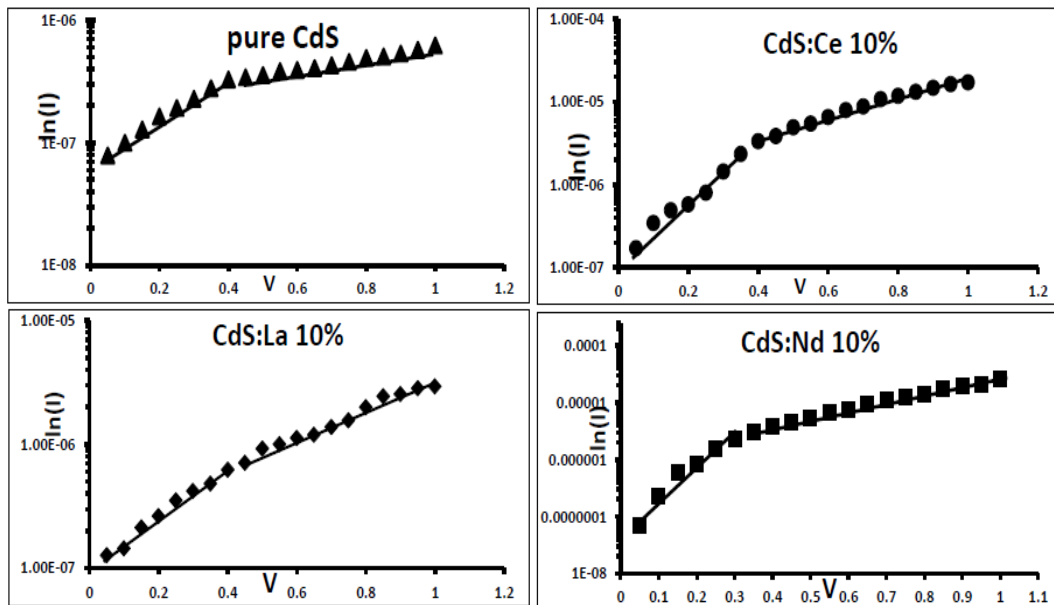

Fig. 7: Variation ln(I) VS Voltage under forward bias in dark for CdS and (Ce, La and Nd) doped CdS at 10 %.

Fig.8 shows the I-V characteristics of CdS/p-Si, CdS:Ce/p-Si, CdS:La/p-Si and CdS:Nd/p-Si at illumination (100 mW/cm^2, 183 mW/cm^2 and 288 mW/cm^2), under forward and reverse bias, which explained the higher magnitude of the current compared with dark, this increasing refer to absorption of light by the samples and generates extra charge carriers contributed increase photocurrent, and this increase also due to an increase in conductivity and resistivity decreases. The excitations of valence electrons into the conduction band significantly improve the electrical conductivity of

the semiconductors. Therefore, observing the variation in the I-V plots with respect to the intensity with which

the optimized samples were illuminating suggests that CdS films exhibits photocurrent detector.
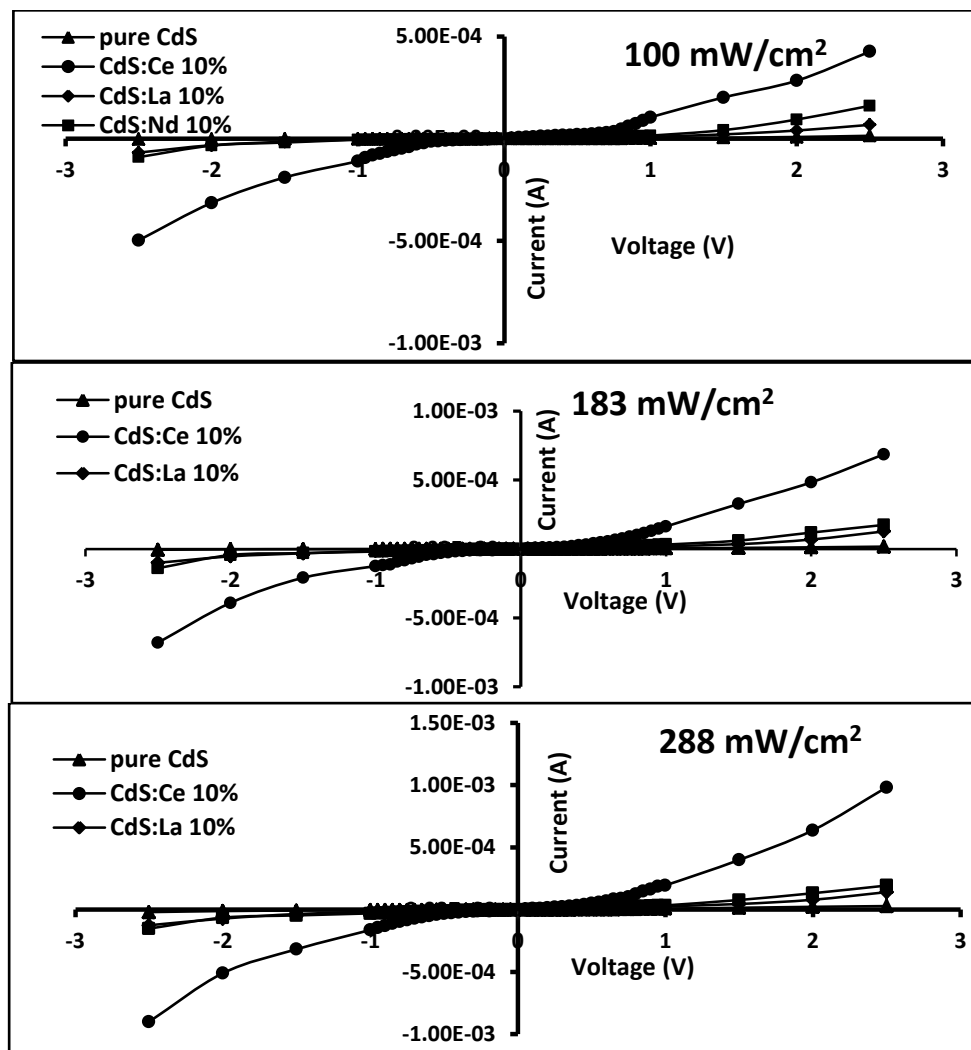

Fig.8: I-V characteristics of CdS and (Ce, La and Nd) doped CdS at 10% in light condition.

Conclusions

Pure CdS and (Ce, La and Nd) doped CdS thin films with concentration 10% have been synthesized by chemical Spray Pyrolysis Method. XRD pattern shows the formation of hexagonal phase and approves the incorporation of (Ce, La and Nd) due to shift those peaks toward lower angle. FESEM images confirmed the surface is covered by big grains with a triangular shape, the optical measurements explain enhancement in transmission and optical band gap which illustrates quantum confinement effect, also

photoluminescence increase in case of doping with rare earth elements compare with pure CdS. The current-voltage characteristics shows increase in photocurrent and dark current in forward and reverse biases, and this increasing occur with (Ce, La and Nd) doped CdS. All the results showed that the cerium doped CdS are the best in improving structural and optical properties.

References
[1] S. Khajuria, S. Sanotra, H. Khajuria, A. Singh, H. N. Sheikh, Acta. Chim. Slov., 63 (2016) 104-112.

[2] R. Banerjee, R. Jayakrishnan, P. Ayyub, J. Phys. Condens. Matter, 12 (2000) 10647-1065.

[3] C. Ricolleau, L. Audinet, M. Gandais, T. Gacoin, Eur. Phys. J. D., 9 (1999) 565-570.

[4] K. Deshmukh, M. Mukherjee, S. Bhushan, R.C. Agrawal, Recent Research in Science and Technology, 4, 8 (2012) 55-57.

[5] D. Govindarajan and C. K. Nithya International Journal of Scientific & Engineering Research, 5, 12 (2014) 427-430.

[6] M. Keikhaei, L. Motevalizadeh, E. A. Kakhki, International Journal of Nanoscience, 15, 3 (2016) 1-5.

[7] P. Urquhart, IEE Proceedings J. Optoelectronics, 135, 6 (1988) 385-402.

[8] Hang Li "Structural and Optoelectronic Properties of Rare Earth Doped Silicon Photonic Materials". PhD thesis, University of Manchester, Faculty of Engineering and Physical Sciences, UK, 2013.

[9] H. J. Lozykowski and W.M. Jadwisienkzak, J. Appl. Phys., 88 (2000) 210-222.

[10] S. Bhushan and A. Oudhia, Indian Journal of Pure & Applied Physics, 47 (2009) 60-65.

[11] S. Agrawal and A. Khare, Arabian Journal of Chemistry, 8, (2015) 450-455.

[12] L. Saravanan, A. Pandurangan, R. Jayavel, Mater. Lett., 66 (2012) 343-345.

[13] K. Deshmukh, M. Mukherjee, S. Bhushan, Turk J. Phys., 36 (2012) 9-21.

[14] L. Saravanan, R. Jayavel, A. Pandurangan, Liu Jih-Hsin, Miao Hsin-Yuan, Materials Research Bulletin, 52 (2014) 128-133.

[15] M. E. L. Avilés, J. I. C. Rascón, J. D. Reyes, J. M. Juárez, R. S. C. Ojeda, M. G. Arellano, J. A. B. Lopez, M. Á. Ramos, Materials Research, 21, 2 (2018) 1-11.

[16] M. Sreenivas, G.S. Harish, P. Sreedhara Reddy, International Journal of Advanced Research, 2, 11 (2014) 468-472.

[17] S. Yılmaza, S.B. Törelib, İ. Polatc, M.A. Olgard, M. Tomakine, E. Bacaksızd, Materials Science in Semiconductor Processing, 60 (2017) 45-52.

[18] M. Tomakin, Y. Öncel, E.F. Keskenler, V. Nevruzoğlu, Z. Onuk, O. Görür, Journal of Alloys and Compounds, 616 (2014) 166-172.

[19] P. Verma, S. G. Manoj, A. C. Pandey, Physica B: Condensed Matter, 405, 5 (2010) 1253-1257.

[20] A. Podesta, N. Armani, G. Salviati, N. Romeo, A. Bosio, M. Prato Thin Solid Films, 511-512 (2006) 448-452.

[21] T. Hurma, Optik, 127 (2016) 10670-10675.

[23] S. Yılmaz, Applied Surface Science, 357 (2015) 873-879.

[23] A. S. Hameed, AL-Bahir Quarterly Adjudicated Journal for Natural and Engineering Research and Studies, 6, 11-12 (2017) 25-32.

[24] S. K. Mishra, R. K. Srivastava, S.G. Prakash, R. S. Yadav, A.C. Panday, Journal of Alloys and Compounds, 513 (2012) 118-124.

[25] M. A. Mahdi, J. J. Hassan, S. S. Ng, Z. Hassan, N. M. Ahmed, Physica E, 44 (2012) 1716-1721.

[26] R. Kumar, R. Das, M. Gupta, V. Ganesan, Super lattices and microstructures, 59 (2013) 29-37.

[27] T. Sivaraman, A.R. Balu, V.S. Nagarethinam, Mater. Sci. Semicond. Process., 27 (2014) 915-923.

[28] A.Green, "Solar Cells", translated by Y. Hassan, University of Mosal P. 102, 1989.

[29] Eman M. Nasir, International Journal of Engineering and Advanced Technology (IJEAT), 3, 2 (2013) 425-429.